Spreading of complex fluids with a soft blade

Marion Krapez,[1] Anaïs Gauthier [●],[1] Jean-Baptiste Boitte,[2] Odile Aubrun,[2]
Jean-François Joanny [●],[3,4] and Annie Colin [●][1]

[1]*MIE–Chemistry, Biology and Innovation (CBI) UMR8231, ESPCI Paris, CNRS,
PSL Research University, 75794 Paris, France*
[2]*Centre de recherche de l'Oréal, 94550 Chevilly-Larue, France*
[3]*Physico Chimie Curie, Institut Curie, PSL University, 75005 Paris, France*
[4]*Collège de France, 75005 Paris, France*

The spreading of complex fluids is not only a part of our everyday life but also a central process in industry to produce functional thin films or protective coatings. Here we consider the spreading of polymer solutions with an elastic blade that deforms during the coating (similarly to a brush or a finger). By using complex fluids with well-chosen rheological properties, we disentangle the effects of shear viscosity, shear thinning, and normal stresses. We reveal two counterintuitive results: First, the mechanical work needed to spread a given volume of a shear-thinning fluid is higher than for the same volume of an equivalent Newtonian fluid at constant spreading velocity. Second, the first normal stress difference, which usually leads to remarkable behaviors such as the swelling of jets or the rise of the fluid on a rotating rod, has strikingly negligible effect here.

I. INTRODUCTION

Many industrial situations require the deposition of a uniform liquid film on a substrate either to produce a functional thin film [1–4] or a protective coating (glass treatment, cosmetics, paint, etc.). The fluid can be deposited directly by drawing the substrate out of a liquid bath (*dip coating*) or with the help of a nondeformable solid [5] or an elastic solid tool, a technique we call here *blade coating*. Interestingly, an analogy is often made between the physics of dip coating and blade coating. In dip-coating experiments, the thickness of the film is set by the deformation of the liquid bath surface close to the substrate. The static meniscus is deformed into a dynamic meniscus, which shape and curvature is set by a competition between capillary and viscous forces [6,7]. Soft blade coating is currently viewed as an "elastic" dip-coating problem [8–11] where elastic forces due to the bending of the blade resist the viscous force and replace the capillary forces. These studies deal with infinite reservoirs, the blade is always totally covered by the liquid. Recent experiments on Newtonian fluids [12] have shown that this analogy is fragile when the size of the reservoir is finite. The deposited thickness diminishes with time as the fluid reservoir below the blade empties. The film thickness seems to be fixed by the length of the blade wet by the liquid and not by the size of a dynamic "elastic meniscus" due to the deformation of the moving blade. However, these experiments are performed on a restricted range of parameters, which limits the validation of the scaling laws. Here we propose to use complex fluids with well-characterized shear-thinning behavior and first normal stress difference to probe with precision the flows. This allows us to conclude definitively on the possible analogy between dip coating and blade coating. In addition, this approach is also important from an industrial point of view: In most formulations (as in paint and cosmetic creams), at least a small amount of polymer is added to the liquid [13], and its influence on the spreading is not known.

Strikingkly, we highlight counterintuitive behaviors. First, it requires a higher mechanical work to spread a shear-thinning fluid than a Newtonian fluid—for an identical initial fluid volume, blade velocity, and spreading duration. Second, normal forces, known to create instabilities and swellings of the deposits during dip coating [14], play little or no role in blade spreading.

The organization of the manuscript is as follows. After presenting the fluids used and our experimental setup (Sec. II), we show experimentally how the fluid rheology impacts the film thickness (Sec. III) and model our results by combining a scaling law analysis and simulations (Sec. IV). We finally discuss how the fluid rheology impacts the spreading process (Sec. V).

II. MATERIALS AND CHARACTERIZATIONS

A. Formulation and rheological properties of the solutions

Three different fluids are used in the experiments: (i) a Newtonian silicone oil (Sigma Aldrich, 500 cSt) with viscosity $\eta = 480$ mPa s; (ii) a shear-thinning solution of xanthan gel (Rhodicare XC, Solvay) (this is made by dissolving 0.9% in mass of polymer in pure water under mechanical agitation), and 0.5% in weight of 2-phenoxyethanol is eventually added as a biocide; and (iii) solutions of partially hydrolyzed polyacrylamid polymer (HPAM, from SNF Floeger) with a high molar mass $M_w = 18 \times 10^6$ g/mol, which are known to generate important normal stress. The polymer is dissolved in water through gentle magnetic agitation to produce solutions with concentrations 0.1%, 0.3%, and 0.5% in weight. Before use, all the polymer solutions are kept at rest for 24 h.

The flow curve of the formulations is obtained using a rheometer (DHR-2, TA) equipped with a cone and plate cell, with radius $R = 20$ mm and angle $\alpha = 2°$. The rheometer imposes a torque T on the rotational axis and measures the angular velocity of the axis ω and the normal force F exerted on the cone by the fluid. As is done classically, the mean shear rate $\dot{\gamma}$ is calculated from ω, with $\dot{\gamma} = \omega/\tan(\alpha)$, the mean shear stress σ is deduced from the torque $\sigma = \frac{3T}{2\pi R^3}$. These definitions ensure that $(\sigma, \dot{\gamma})$ correspond to the mean of the local shear stress $\sigma(r)$ and the mean of the local shear rate $\dot{\gamma}(r)$ in the Newtonian fluid situation. The first normal stress difference N_1 born by the sample is calculated from the vertical force F, with $N_1 = \frac{2F}{\pi R^2}$. It is corrected for inertia, which is not negligible at angular velocities $\dot{\gamma} > 10^2$ s^{-1}, with $N_1^{\text{inertia}} = -\frac{3\rho\omega^2 R^2}{20}$ (denoting ρ the fluid density).

In most experiments, a computer-controlled feedback loop on the torque T is used to keep a constant angular velocity (hence a constant mean shear rate) without any fluctuations ($\frac{\delta\dot{\gamma}}{\dot{\gamma}} < 0.001$). The temperature is set to 298.15 ± 0.1K using a water circulation around the cell. The flow curves are obtained using a shear-imposed flow-sweep, with five points per decade. The stress value is given when three consecutive 10-s-long measurements have given the same results with 5% tolerance or when the sample has undergone 60 s of constant shear rate. This maximum time is long enough to ensure that the measurements are not sensitive to the inertia of the rheometer.

Figure 1(a) presents the flow curves of the fluids considered here. As expected, silicone oil (shown with red squares) is Newtonian, with a constant viscosity η (independent on $\dot{\gamma}$). The solutions of xanthan gum (blue circles) and HPAM (green triangles), however, are all shear thinning. Their viscosity follow a classical empirical law for polymer solutions:

$$\eta = \begin{cases} \eta_0 & \text{for } \dot{\gamma} < \dot{\gamma}_c \\ k\dot{\gamma}^{n-1} & \text{for } \dot{\gamma} > \dot{\gamma}_c \end{cases}, \tag{1}$$

Interestingly, the 0.9% xanthan and the 0.5% HPAM solutions have almost the same viscosity at all the shear rates considered here: The curves $\eta = f(\dot{\gamma})$ overlap. There is, however, a major difference between these two fluids, as shown in Fig. 1(b). In both fluids, the first normal stress difference N_1 follows the law $N_1 = \alpha\dot{\gamma}^m$, but the 0.5% HPAM solution display an important first normal stress difference, contrary to the 0.9% xanthan solution. This is evidenced in the inset of Fig. 1(b): Normal stresses cause the swelling of a 0.5% HPAM jet (green), a phenomenon that is not observed for xantan (blue). The values of the parameters η_0, n, k, α, and m for all the suspensions are given in Table I.
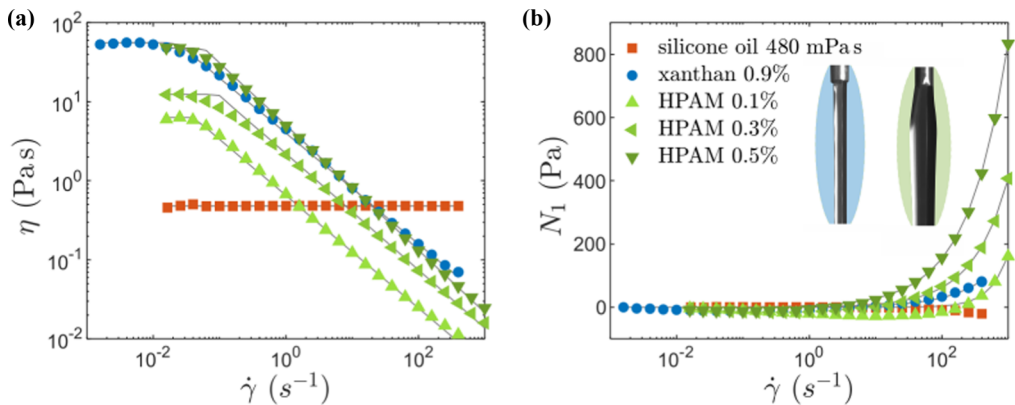
FIG. 1. Rheological curves of silicone oil with viscosity $\eta = 480$ mPa s, xanthan gum at 0.9% and HPAM solutions with concentrations 0.1%, 0.3%, and 0.5%. (a) Viscosity η as a function of the shear rate $\dot{\gamma}$. (b) First normal stress difference N_1 as a function of $\dot{\gamma}$. The pictures show the swelling of a jet of HPAM at 0.5% (green) compared to xanthane at 0.9% (blue) from a capillary tube of outside diameter 0.65 mm and at a flow rate of 0.5 ml s^{-1}.

B. Experimental device

The blade coating experiment is presented in Fig. 2(a). The fluid is spread with a soft blade, made of a rectangular plastic sheet of Mylar, with thickness $u = 125$ μm, width $b = 4$ cm and length $L = 5.7$ cm. The modified Young modulus $E^* = \frac{E}{1-\nu^2}$ of the sheet (which includes the Poisson ratio ν) is equal to 6.2 ± 0.6 GPa. It is determined by measuring the deflection under its own weight, following Refs. [12,15].

The blade is clamped vertically above a PMMA substrate, at a height $y = 0.46L$. This height is chosen so that the tip of the blade is just tangent to the substrate in absence of liquid [8]. Both the blade and the substrate are sanded to avoid a potential dewetting and slippage. The roughness of the blade and the surface is of the order of 5 μm, which is at least one order of magnitude smaller than the thickness of the deposit. A known volume of liquid Ω_0 (between 0.05 and 1.3 cm^3) is deposited under the blade and spread in a one-way movement by sliding the substrate at a constant velocity $V = 1$ cm/s over 10 cm. The film thickness $e(t)$ is measured 2 mm beyond the tip of the blade using an optical profilometer. Simultaneously, the amount of liquid wetting the blade at a given time t is measured thanks to a camera placed above the translucent mylar sheet. It is quantified by the wetting length l_w, which measures the portion of the blade that is in contact with the liquid [Fig. 2(a)].

TABLE I. Rheological properties of xanthan gum and HPAM solutions.

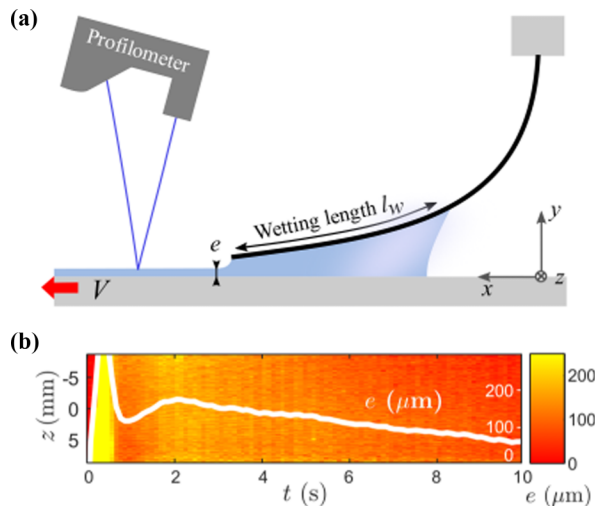|	Xanthan	HPAM		
	0.9%	0.1%	0.3%	0.5%
η_0 (Pa s)	56	6.3	12.4	48
k	4.0	0.65	2.2	5.1
n	0.30	0.29	0.27	0.21
α	0.99	2e-3	1.44	5.24
m	0.74	1.62	0.82	0.73

FIG. 2. (a) Schematic representation of the soft blade coating experiment. (b) Map of the central part of the film for xanthane 0.9% during the spreading, as a function of the width z and time t. The color code varies from $e \simeq 0$ (red) up to $e = 250$ μm (yellow). The first peak is an artifact and is not taken into consideration. The white line shows the mean thickness $e(t)$ over the film width as a function of time.

III. EXPERIMENTAL RESULTS

Figure 2(b) displays the temporal evolution of e along the z axis (with $z = 0$ the center of the blade) as a function of time. The fluid used is xanthan gum, with an initial volume $\Omega_0 = 0.58$ ml. As evidenced by the white line, which plots the mean value of $e(t)$ along the z axis, the film thins out during the course of an experiment. After a transient state (corresponding to the first two seconds), the film thickness $e(t)$ continuously decreases, from 175 to 20 μm at the end of the 10-s-long blade movement. This a consequence of the finite size of the liquid reservoir below the blade. Indeed, and as shown in Fig. 3, $e(t)$ is a function of the wetting length $l_w(t)$, measured at the same time. This observation is valid for all liquids used in the experiment: Figure 3(a) which displays the overlap of more than 30 experiments in total [an experiment corresponds to a set of values $e(t)$, $l_w(t)$]. Interestingly, as highlighted in Fig. 3(b), the measurements obtained with the 0.5% HPAM solution are almost identical to those obtained with the 0.9% xanthan gum solution. Even if these two fluids share the same rheological curve [in Fig. 1(a), the viscosity $\eta(\dot{\gamma})$ of HPAM overlaps the data points of xanthan], the first normal stress difference in HPAM reaches several hundreds of pascals under high shear [Fig. 1(b)] while N_1 is always smaller than 80 Pa in xanthan. Under the conditions of the spreading experiments, one would naively expect the normal stress to play a role: Indeed, the Weissenberg number $\mathrm{Wi} = \frac{N1}{\tau} \sim \frac{\alpha}{k}(\frac{V}{e})^{m-n}$, which compares the first normal stress difference N_1 to the shear stress τ, is around 1 in the case of xanthan gum solutions, whereas it is about 10 in the case of HPAM solutions. This indicates that in our experiments, the normal forces generated by the flow in HPAM are very important compared to the shear stress forces. However, they do not impact the film deposition law.

IV. MODEL

To capture this point and model the relation between e and l_w for the non-Newtonian fluids, we propose a scaling analysis.

In all our experiments, the liquid is highly confined below the blade: The wetting length l_w typically varies between 2 cm and a few millimeters, while e is of the order of 100 μm, so that $l_w \gg e$. The Reynolds number $\mathrm{Re} = \rho e V/\eta$ is smaller than 10^{-1} (denoting $\rho \simeq 10^3$ kg/m^3 the fluid
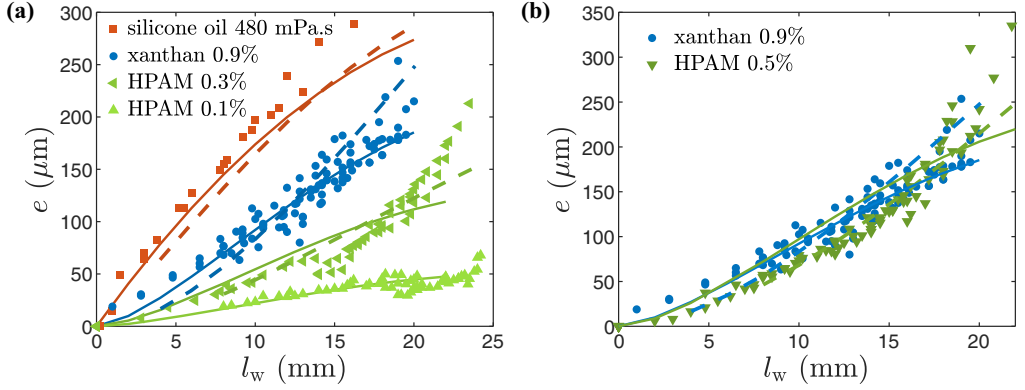
FIG. 3. (a) Evolution of the fluid thickness e with the wetting length l_w for two complex fluids (xanthan 0.9% in blue, HPAM 0.3% in green, and HPAM 0.1% in light green) and a Newtonian fluid (silicone oil, $\eta = 480$ mPa s in red). The markers correspond to the experimental data measured for different initial fluid volumes. The continuous lines show the scaling law [Eq. (1)] with prefactors 0.17 (for silicone oil) and 0.06 (for xanthan and HPAM) corresponding to the best fits. The dashed lines are the numerical solutions. (b) Comparison of xanthan 0.9% and HPAM 0.5% (dark green). The blue symbols correspond to the same experiments in (a) and (b).

density and $\eta > 10^{-2}$ Pa s the fluid viscosity). In addition, the tip of the blade is almost parallel to the substrate, and the mean angle in the wet part of the blade is typically $5°$. This implies that the shear gradient is mostly horizontal and the elongational component of the flow is negligible. Thus, the flow below the blade is close to a simple lubrication flow: The fluid velocity **v** is oriented along the x axis and varies with y only.

In the general case, and when neglecting gravity, the fundamental relation of dynamics at low Reynolds number is

$$\frac{\partial P}{\partial x} = \frac{\partial \tau_{xx}}{\partial x} + \frac{\partial \tau_{xy}}{\partial y} + \frac{\partial \tau_{xz}}{\partial z}, \tag{2}$$

with P the hydrodynamic pressure within the fluid and τ the deviator of the stress sensor (which has the same symmetry as the velocity field). Equation (2) can be expressed as a function of the first and second normal stress differences N_1 and N_2. Using $N_1 = \tau_{xx} - \tau_{yy}$ and $N_2 = \tau_{yy} - \tau_{zz}$ and $\tau_{xx} + \tau_{yy} + \tau_{zz} = 0$ (by definition of the pressure), Eq. (2) is written as follows:

$$\frac{\partial P}{\partial x} = \frac{\partial \tau_{xy}}{\partial y} + \frac{\partial \left(\frac{2N_1+N_2}{3}\right)}{\partial x} + \frac{\partial \tau_{xz}}{\partial z}. \tag{3}$$

In our experiment, symmetry implies that $\tau_{xz} = 0$. In addition, and following Refs. [14] and [16], we consider that $N_2 \ll N_1$, which is classical for polymer solutions. Finally, the steady Stokes equation in the lubrication approximation is

$$\frac{\partial P}{\partial x} = \frac{\partial \tau_{xy}}{\partial y} + \frac{2}{3}\frac{\partial N_1}{\partial x}. \tag{4}$$

The pressure in the liquid film confined below the blade is thus the sum of two terms. The first is the lubrication pressure, which scales as $\tau \frac{l_w}{e}$ (denoting $\tau = \tau_{xy}$) and the second is due to the normal stresses and is proportional to N_1. During the spreading with a soft blade, the pressure generates a lift force, which is balanced by a restoring elastic force coming from the blade. To evaluate the influence of the normal stresses on the spreading, we define a nondimensional number, $\mathcal{E} = \frac{2N_1 e}{3\tau l_w} \sim \frac{2}{3}\mathrm{Wi}\frac{e}{l_w}$, which compares the contributions of the two terms of the total fluid pressure P. In practice, the condition $\mathcal{E} \ll 1$ is always true for the 0.9% xanthan gum solution, which indicates

that the shear-thinning effects are dominant over the elastic effects. Interestingly, it is also verified for the 0.5% HPAM solution, despite a Weissenberg number Wi $\simeq 10$. Indeed, $\mathcal{E} \ll 1$ as long as $l_w > 0.05$ mm, which is always the case in our experiments.

We now propose a scaling law to model the film thickness e. The blade is subjected to two forces: a lift force F_{lift} created by the flow of the fluid which tends to lift the blade from the plate and an elastic restoring force which tends to stick the blade to the plate F_{blade}. If $\mathcal{E} \ll 1$, then the lift force $F \sim (P - Po)l_w b$ (with b the width of the blade) created by the fluid on the blade is mainly given by the increase of pressure $(P - Po)$ due to the confined flow. This value is estimated from Eq. (4). When $\mathcal{E} \ll 1$, we get $\frac{P - Po}{l_w} = \frac{\tau}{e}$ where the tangential stress τ is given by $\tau = k(\frac{V}{e})^n$. The lift force scales thus as $F_{\text{lift}} \sim k(\frac{V}{e})^n \frac{l_w^2 b}{e}$. This force is compensated by the rigidity of the blade, which induces a resisting force $F_{\text{blade}} \sim \frac{E^* I}{(L - l_w)^2}$ (denoting I the second moment of inertia of the blade). This scaling law is found by relying on the equations of elastica [17]. The part of the blade that is not covered by the liquid is in the air. In this situation (i.e., for s between 0 and $L - l_w$), the shape of the blade is given by the following two equations:

$$\frac{d\Gamma}{ds} = (\vec{F} \times \vec{t}) \cdot \vec{u}_z, \tag{5}$$

$$\frac{d\vec{F}}{ds} = 0, \tag{6}$$

where $\vec{F}$ and Γ are respectively the force and the projection of the torque on $\vec{u}_z$ exerted at a point of the blade by the portion of the blade located "on its right," $\vec{t}$ is the vector tangent to the surface, and $\vec{u}_z$ the vector along the width of the blade. This leads to $E \frac{d^2\theta}{d2s} = F_{\text{blade}}$ where θ is the angle between the downward vertical and the tangential vector to the blade. If l_w is less than L, then we can estimate $\frac{d^2\theta}{d^2 s} = \frac{0 - \frac{\pi}{2}}{(L - l_w)^2}$ as θ goes to $\frac{\pi}{2}$ when s goes to L. If l_w is close to L, then we get $\frac{d^2\theta}{d^2 s} = \frac{-\theta}{(L - l_w)^2}$, which differs from the last case as θ goes to 0 when s goes to 0. This point explains why our expression is valid only for l_w less than L and gives $F_{\text{blade}} \sim \frac{E^* I}{(L - l_w)^2}$.

The balance between the two forces sets the film thickness e:

$$e \sim l_w \left\{ \left(1 - \frac{l_w}{L}\right)^2 \left[\frac{k\left(\frac{V}{l_w}\right)^n L^2 b l_w}{E^* I} \right] \right\}^{1/(n+1)}, \tag{7}$$

with the condition $\mathcal{E} \ll 1$, which correspond to $\frac{\alpha}{k}(\frac{V}{l_w})^{\frac{m}{n+1}}(1 - \frac{l_w}{L})^{\frac{2(1-m+n)}{n+1}}(\frac{kL^2 b l_w}{E^* I})^{\frac{1-m+n}{n+1}} \ll 1$.

At first sight this equation is striking since it predicts that e vanishes when l_w goes to zero. We recall that the value of e cannot be deduced from this equation since it is not valid when l_w tends to L, i.e., in the case of an infinite reservoir. This comes from the calculation of the elastic force of the blade which is no longer valid.

For Newtonian fluids, i.e., for $n = 1$, Eq. (7) is similar to the scaling suggested by Krapez *et al.* [12]. In this previous work [12] we have checked the dependence of the scaling law on each of the variables for a Newtonian fluid. We have varied the velocity (four values between 2.5 and 10 mm/s) and the thickness of the blade (between 1 and 7 mN m) and the length of the blade (5.7 and 7 cm) and shown that all the data collapsed. Here we focus on the rheological properties of the fluid and study four non-Newtonian fluids with different rheological laws (the parameters are given in Table I). The effect of speed is analyzed on two different speeds. We anticipate that the wetting conditions and our experimental setup do not allow us to study respectively lower or higher speeds.

In Fig. 3, the scaling law is shown with a continuous line and compared with the experimental data, using the values of n and k extracted from the flow curves (Table I). The experimental data reported correspond to several different films (at least five experiments per concentration). The reported noise is the experimental noise. A prefactor of 0.06 is used for all the shear-thinning fluids and of 0.17 for silicone oil. For $l_w > 15$ mm, the scaling law fits well with the data: It reproduces
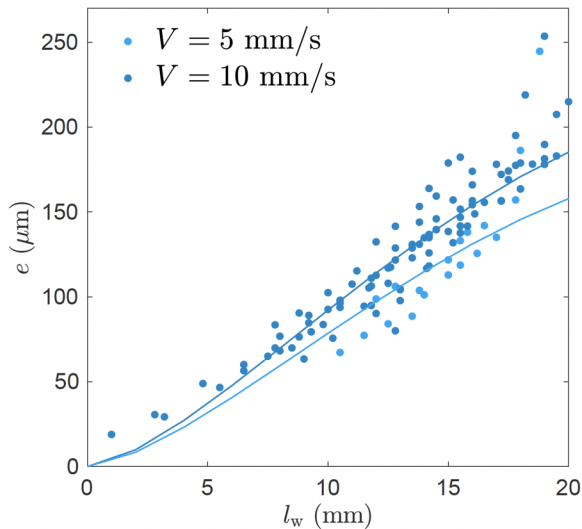
FIG. 4. Evolution of the fluid thickness e with the wetting length l_w for two different velocities and for a solutions of xanthan (and 0.9%). The continuous lines show the scaling law [Eq. (1)] with prefactors of 0.06 corresponding to the best fits.

in particular the dependency of e with l_w and the relative variations of e with the rheology of the fluids. The same agreement is found when the velocity is varied (see Fig. 4).

A sharp increase, however, is observed for large reservoir sizes, typically here for $l_w > 15$ mm that is not predicted by the model. To get a better understanding of this complex situation, we performed a full numerical computation of the experiment. The principle of the computation is detailed in the Appendix. Basically, the spreading dynamics are described using two sets of equations, coupled by boundary conditions at the tip of the blade. The first set of equations models the viscoelastic interaction between the blade and the fluid. It is resolved using Euler's elastica, where the bending torque of the blade is compensated for by the torque arising from the gradient of tangential stress in the lubricated layer of fluid below it. The capillary forces arising from the liquid surface deformation on the left and right parts of the wet area of the blade are included in the boundaries conditions for the pressure p. The second set of equations models the free liquid film at the blade exit. These equations correspond to the canonical Landau-Levich situation: They express the equilibrium between viscosity and surface tension, which sets the behavior of the spread film. The matching between these two sets of equations is done iteratively by imposing the continuity of the flow rate at the tip of the blade. In both sets of equations, the fluid is modelled within the lubrication approximation, taking into account the rheological properties describing the Newtonian or shear-thinning behavior. The values of η_0, k, and n are taken from Table I. The results of the simulation are shown with dotted lines in Fig. 3. They match well the experimental data for all the fluids considered here and without any adjustable parameter. This confirms our dimensional analysis. Deviations are also observed for high values of l_w. We believe that this is due to a bad description of the shape of the back meniscus of the volume of fluid below the blade when l_w is large.

V. DISCUSSION

The simulations, in which the normal stress is neglected, confirm the very little role played by first normal stress in blade spreading experiments: In Fig. 3(b), the plots $e(l_w)$ are nicely reproduced for both xanthan and HPAM. The difference with other classical situations is striking. In general,

these stresses cause spectacular effects, such as a swelling of the fluid flowing out of a tube in extrusion processes, or the climbing of the fluid along rotating rods [18]. Here, contrary to most flows, the Weissenberg number is not the appropriate characteristic number to characterize the normal stress effects in spreading experiments, and a new number $\mathcal{E} = \frac{2}{3}\text{Wi}\frac{e}{l_w}$ has to be defined. In our experiment, even if the Weissenberg number is close to 10 in the 0.5% HPAM solution—which indicates that the first normal stress difference dominates over the shear stress—$\mathcal{E}$ is of the order of 0.1 due to the geometrical factor $\frac{e}{l_w} \simeq 10^{-2}$. This explains why the effect of normal stresses is negligible in soft blade spreading. This geometrical factor is central to explain the difference with other experiments. For example, de Ryck *et al.* [14] evidence a very strong effect of the normal stresses when dip coating a fiber. They use a 1% PAA solution with properties similar to the 0.5% HPAM solution so that the Weissenberg number is also close to 10. However, in dip coating, the characteristic length scale in the x direction is an internal length $l \sim \sqrt{eb}$ with b the thickness of the fiber. In Ref. [14] the ratio e/l varies between 0.2 and 1 so that $\mathcal{E}$ is always larger than 1. In our experiment, however, the presence of the blade imposes the wetting length l_w as the relevant horizontal length scale. Since $l_w \simeq 100\,e$, we cannot observe any effect of the normal stresses unless the Weissenberg number is larger than 100, a situation that cannot be obtained with the fluids used here and which will be difficult to achieve.

However, it is important to note that even if the normal stresses play no role here, the shear-thinning rheology of the fluids has a strong influence on blade coating. To evidence this point, we compare the spreading process of shear-thinning and Newtonian fluids, focusing on the work needed to spread the fluid and the film profile

First, it is necessary to carefully select the viscosity of the "equivalent" Newtonian fluid that is compared with a given shear-thinning solution. To do so, we do the following thought experiment: Starting with identical initial conditions (same initial amount of fluid below the blade; i.e., same l_{wi}, same spreading velocity V), it should take the same time t_d to spread a volume Ω_d of the equivalent Newtonian fluid than the shear-thinning fluid of interest. Indeed, if the mechanical properties of the blade are known, then, for a fixed V and l_{wi}, there is a bijective relation between the spreading time and the viscosity of the Newtonian fluid. Figure 5(a) illustrates the choice of the equivalent Newtonian fluid for the 0.9% xanthan solution. Using the simulations, we plot (with a continuous line) the time t_d necessary to spread a given volume Ω_d of xanthan. With dotted lines, we show the spreading time $t_d(\Omega_d)$ for four different Newtonian fluids, with viscosity $\eta = 150, 300, 500,$ and 1000 mPa s. As evidenced in Fig. 5(a), the equivalent Newtonian fluid has a viscosity $\eta = 300$ mPa s: It almost overlaps the xanthan curve and has an identical spreading time $t_d = 6$ s for $l_{\text{wi}} = 18$ mm and $\Omega_d = 0.40$ cm^3.

To evaluate energy dissipation in blade spreading, we focus on work dissipated by the liquid during the spreading $W = \int_0^{t_d} FV\,dt$ and compare the 0.9% xanthan solution to its "equivalent" Newtonian solution. We denote here F the force exerted by the fluid on the surface (calculated by integrating the shear stress at the liquid/substrate interface in the x and z directions) and t_d the deposition time. The calculated work is negative. It corresponds to the work dissipated by the fluid. To spread the fluid, the experimenter needs to bring $-W$. Figure 5(b) shows the calculated value of W for the 0.9% xanthan solution, the equivalent Newtonian fluid ($\eta = 300$ mPa s), and four others (with viscosity $\eta = 50, 150, 500,$ and 1000 mPa s). We observe that the energy needed to spread the shear-thinning solution is typically 30% higher than its Newtonian equivalent (e.g., 34% for $\Omega_d = 0.40$ cm^3). This result might seem counterintuitive: Indeed, in industrial applications, the addition of polymer to a product is often seen as a way to make the liquid easier to spread. We show here that the opposite happens: Shear-thinning fluids resist more to the spreading than an equivalent Newtonian fluid.

Note that in Fig. 5(b) the xanthan curve is superimposed on the curve of a Newtonian fluid of viscosity 150 mPa s. This means that the same amount of work is needed to spread an equivalent volume of xanthan and a fluid with viscosity 150 mPa s. However, the deposition time is longer for the fluid of viscosity 150 mPa s than with xanthan [Fig. 5(a)]. It is thus not a Newtonian equivalent in our definition, as opposed to 300 mPa s.
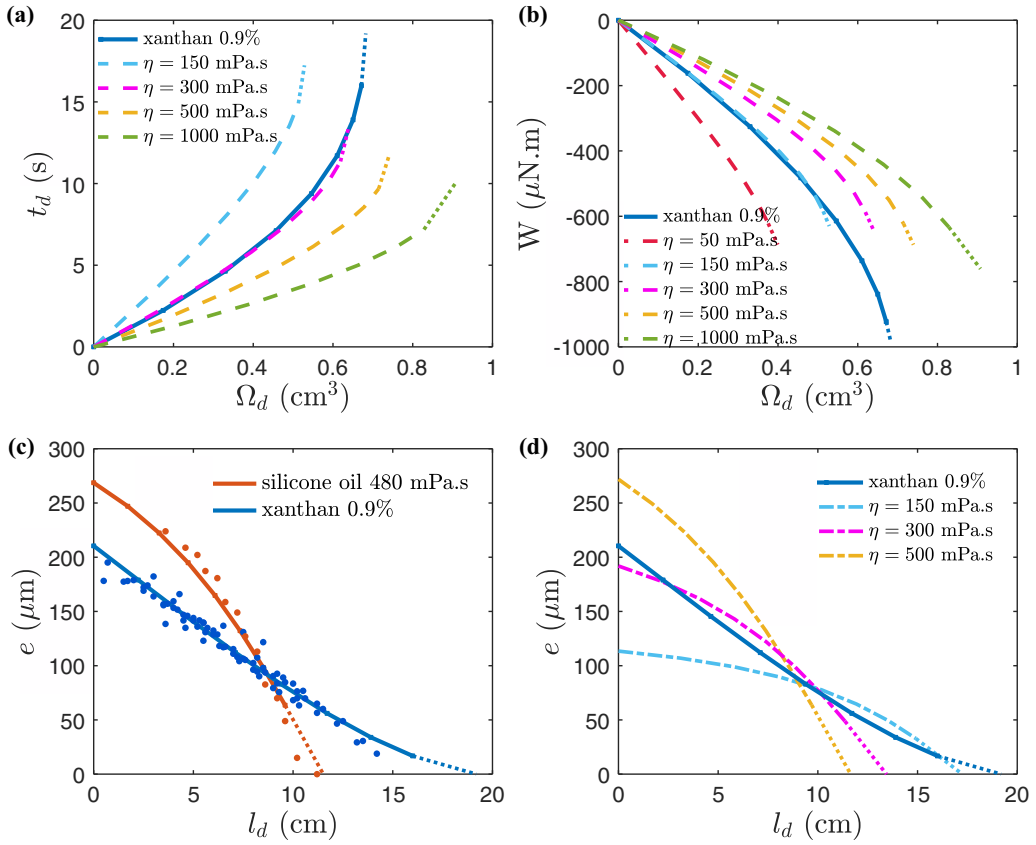
FIG. 5. (a) Deposition time t_d as a function of the deposited volume Ω_d for xanthan at 0.9% (dark blue) and Newtonian fluids with viscosity from top to bottom: 1000 mPa s (green), 500 mPa s (yellow), 300 mPa s (pink), and 150 mPa s (cyan). For $\Omega_0 = 0.40$ cm^3, $t_d = 6$ s for the xanthan solution. (b) Work of the viscous forces during the spreading of volume Ω_d for the fluids of Fig. 5(a) and 50 mPa s (red). The xanthan fluid dissipates more energy than the Newtonian fluid at $\eta = 300$ mPa s. (c) Evolution of the thickness of the deposit as a function of the deposited length for silicone oil of 480 mPa s (red) and xanthan at 0.9%. Dots are experiments, and lines computations without fitting parameters. The experiments are carried with a velocity equals 1 cm s^{-1}. (d) Shape of deposit for xanthan and Newtonian fluids of viscosity: 500, 300, and 150 mPa s.

Another property of the shear-thinning rheology is to change the profile of the deposited film. This is illustrated in Fig. 5(c), where the film thickness e is plotted as a function of the length l_d of the deposited film for two fluid categories. The dots correspond to the experimental data (in red, a Newtonian fluid, silicone oil with viscosity $\eta = 480$ mPa s and in blue a shear-thinning 0.9% xanthan solution). The lines show the result of the simulations. Note that the length of fluid deposited is only modeled in the steady state. To account for this phenomenon, an offset on l_d must be added to the experimental curves to compare the model and the data. In the Newtonian situation, the film thickness drops sharply to zero at the end of the film (when the reservoir is almost empty), here for $l_d = 7, 5$ cm. However, for shear-thinning fluids, the deposited thickness generally decreases more slowly and continuously from the beginning of the process to the end. This experimental observation is confirmed by the simulations shown in Fig. 5(d): The shear-thinning solution (xanthan, in blue) thins out almost linearly, in contrast to its Newtonian equivalent ($\eta = 300$ mPa s). Spreading a shear-thinning fluid results in a more regular and longer film.

VI. CONCLUSION

As mentioned in the Introduction, we study in this work the spreading of complex fluids by a flexible blade and we focus on the case where the volume of liquid is finite. This case is found in particular during the spreading of a paint by a pin or of glue with a flexible squeegee or glue with a flexible squeegee. Most of the articles in the literature [8,13,19–26] concern studies where the liquid reservoir is infinite and we are not aware of published data in the situation of a finite reservoir. We have therefore developed an experimental approach to compare numerical simulations, scaling laws, and experiments. By combining experiments with a judicious choice of fluids, and numerical and scaling law models, we give a better understanding of the spreading dynamics of non-Newtonian fluids. In particular, we show that the thickness of the deposit can be predicted as a function of the rheological features of the fluid. Interestingly, we evidence that shear-thinning fluids require more work to be spread than Newtonian fluids but that the deposit thins out more regularly. These results will be valuable in applications, for example to determine whether a polymer needs to be added to a product or to choose the polymer depending on the expected effect: a thicker or a more regular film or a fluid that is more easy to spread.

Interestingly, we also show that normal stresses play only a small role in the spreading process by a soft blade even if the Weissenberg number is of the order of 10. This implies that the analogy that is often made between soft blade coating and dip coating [8–11] is not valid when the reservoir is infinite. Both processes do not involve the same characteristic length scale: an externally imposed length in blade coating (the wetting length l_w) versus an internal length (the meniscus deformation) in dip coating.

APPENDIX: NUMERICAL SOLUTION OF THE ELASTOHYDRODYNAMIC EQUATIONS

We present in this section the equations used to calculate numerically the blade shape and the flow in a soft blade coating experiment. The general principle is the same as in our previous work [12] but here for a shear-thinning fluid. In particular, the shear-rate dependency of the viscosity implies a different set of equations to describe the fluid contribution (the lubrication pressure and the viscous drag force). The shear-thinning fluid is modelled as in Eq. (1) of the main part of the manuscript: Its viscosity is constant at low shear, and it follows a power law at high shear.

The blade and fluid are described using two sets of equations. The first set, called the "blade equations" [Eqs. (A14), (A17), (A19), (A20), and (A24)], describes the interaction between the elastic blade and the hydrodynamic forces arising from the fluid sheared below it. The second set, the "free surface equations" [Eqs. (A29) and (A31)], describes the free film after the tip of the blade. Finally, we detail the numerical resolution method. Its originality is to rely on an analogy between the hydroelastic equations and the stationary heat transfer equation to solve the problem.

1. Blade equations

We consider in this part the interaction between the blade and the liquid. As shown in supplementary Fig. 6(a), we consider an elastic blade submitted to nonuniformly distributed forces, due to the presence of the shear-thinning liquid below. Since the Reynolds number $\mathrm{Re} = \rho e V / \eta < 10^{-1}$ in the flow is small and since the mean angle between the tip of the blade and the substrate is of a few degrees, we consider that the fluid flow corresponds to a simple Stokes flow in the lubrication approximation. In particular, any elongational component of the flow is neglected.

When the blade is in motion, the fluid flow induces two forces that are distributed nonuniformly along the part of the blade wet by the liquid. We distinguish here a lift force (perpendicular to the blade), due to the lubrication pressure p, and a viscous force f_v (tangent to the surface) arising from the no-slip boundary condition. In addition, we consider the effect of surface tension forces which are tangent to the meniscus at the positions $s = s_w$ and L. As discussed with Newtonian fluids [12], these local forces have a very small impact on the film deposition (the order of magnitude of torque from local capillary forces is 0.1% of the torque resulting from the lubrication pressure). However,
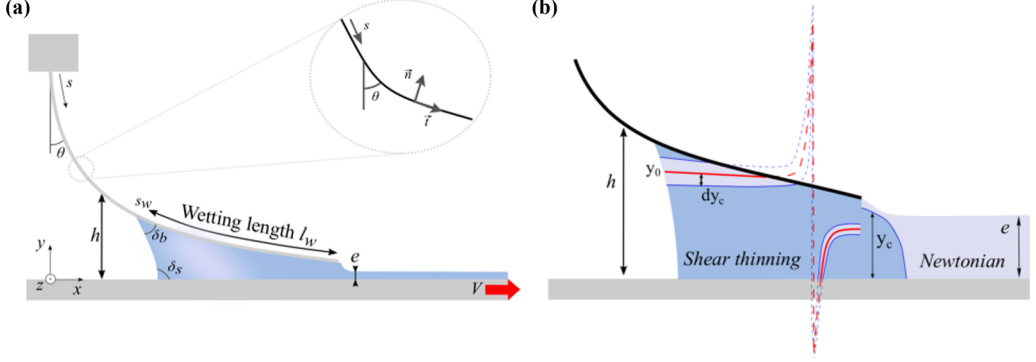
FIG. 6. (a) Soft blade coating experimental setup, notations, and axes convention. (b) Schematic representation of the Newtonian and shear-thinning areas in the liquid.

we still consider the contribution of the Laplace pressure arising from the curvature of the interfaces at $s = s_w$ and $s = L$, which acts as a boundary condition on the lubrication pressure p.

To model the shape of the blade, we use the curvilinear length s along the blade, with $s = 0$ the clamping position and $s = L$ the free edge. The blade is modelled as a large deflection problem, where the normal $\vec{n}$ and tangent $\vec{t}$ vectors [as defined in Fig. 6(a)] both depend on s. We solve the beam equation following a classical method [27]. We consider the variation of the internal torque Γ of the blade with s, which depends on the sum of all the forces exerted on the right of the point of interest s.

By taking into account the lubrication, viscous forces, and capillary forces, the total external force $F(s)$ acting on the right of s on the blade is

$$\vec{F}(s) = \int_s^L [p(s')n(\vec{s}') + f_v(s')t(\vec{s}')]b\,ds' + \vec{F}_c, \tag{A1}$$

where b is the width of the blade and F_c is the capillary force.

Calculation of the forces

Fluid pressure. We model the flow below the blade as a steady flow in the lubrication approximation. We neglect the effect of a potential recirculation near s_w, as well as the first and second normal stress difference. Within this frame, the fluid pressure does not vary with y, and gravity is neglected. The flow equation reads:

$$\frac{\partial \tau}{\partial y} = \frac{\partial P}{\partial x}. \tag{A2}$$

To model the shear-thinning fluid, we use the following equations:

$$\tau = \begin{cases} \eta_0 \dot{\gamma} & \text{for } \dot{\gamma} < \dot{\gamma}_c \\ k|\dot{\gamma}|^{n-1}\dot{\gamma} & \text{for } \dot{\gamma} > \dot{\gamma}_c \end{cases} \tag{A3}$$

Depending on the local shear rate in the flow, the liquid behaves as a Newtonian fluid (when $|\dot{\gamma}| < |\dot{\gamma}_c|$) or as a power-law fluid (when $|\dot{\gamma}| > |\dot{\gamma}_c|$), as evidenced in supplementary Fig. 6(b). In addition, we have to take into account that $\dot{\gamma}$ and the pressure gradient can be negative in some parts of the liquid, and that the power-law index n is inferior to 1. Thus, several cases have to be considered at the same time.

To determine the fluid equations, we define y_0 such as $\tau(y_0) = 0$, which marks the separation between positive and negative shear rate. The vertical asymptotic observed in y_0 corresponds to the position of the maximum fluid pressure which implies a constant shear stress over y. The integration

of Eq. (A2) over y gives:

$$\tau = \frac{\partial P}{\partial x}(y - y_0). \tag{A4}$$

To calculate the pressure in the reservoir we consider the continuity of the shear rates at the limit between the shear-thinning and Newtonian regions. We define dy_c the half width of the area where the shear rate is below $\dot{\gamma}_c$ and the shear stress is expressed as Newtonian [Fig. 6(b)]. The Newtonian region is symmetrical around the y_0 limit as expected from the Stokes equation. We obtain:

$$\frac{\partial P}{\partial x}\frac{dy_c}{\eta_0} = \left\langle \frac{\partial P}{\partial x}\frac{dy_c}{k} \right\rangle^{1/n}. \tag{A5}$$

Note that the notation $\langle x \rangle^a = \text{sgn}(x)|x|^a$ is used in the equations.

Rewriting this equation gives an expression for the pressure gradient, but the sign still needs to be determined:

$$\frac{\partial P}{\partial x} = \text{sgn}\left(\frac{\partial P}{\partial x}\right)\frac{1}{dy_c}\frac{\eta_0^{\frac{n}{n-1}}}{k^{\frac{1}{n-1}}}. \tag{A6}$$

To calculate dy_c, we use Eq. (A3) (expressed as a function of the velocity, by using $\dot{\gamma} = \frac{dv}{dy}$) and combine it with Eq. (A4). The shear rate is then integrated over y with no-slip boundary conditions at the moving plate [$v(0) = V$] and at the blade [$v(h) = 0$]. At the position $y = y_0 \pm dy_c$ we use the continuity of the velocity. Finally, we obtain a set of equations describing the velocity in the different part of the fluid and the flow rate q is calculated by integrating v over y. A general equation for the linear flow rate is obtained as follows:

$$q = Vy_0 - \frac{1}{3\eta_0}\left\langle \frac{\partial P}{\partial x} \right\rangle (\text{sgn}(y_0)\min(|y_0|, dy_c)^3 + \text{sgn}(h - y_0)\min(|h - y_0|, dy_c)^3) + \left\langle \frac{1}{k}\frac{\partial P}{\partial x} \right\rangle^{1/n}$$

$$\times \left[\frac{-\langle y_0 \rangle^{1/n+2} - \langle h - y_0 \rangle^{1/n+2} + \text{sgn}(y_0)\min(|y_0|, dy_c)^{1/n+2} + \text{sgn}(h - y_0)\min(|h - y_0|, dy_c)^{1/n+2}}{1/n+2} \right]. \tag{A7}$$

The sign of $\frac{\partial P}{\partial x}$ is the same as $Vy_0 - q$ [result obtained from Eq. (A7)] which gives:

$$\frac{\partial P}{\partial x} = \text{sgn}(Vy_0 - q)\frac{1}{dy_c}\frac{\eta_0^{\frac{n}{n-1}}}{k^{\frac{1}{n-1}}}. \tag{A8}$$

By writing the condition of velocity continuity at y_0 we obtain another equation:

$$0 = V - \frac{1}{2\eta_0}\left\langle \frac{\partial P}{\partial x} \right\rangle [\min(|y_0|, dy_c)^2 - \min(|h - y_0|, dy_c)^2]$$

$$- \left\langle \frac{1}{k}\frac{\partial P}{\partial x} \right\rangle^{1/n} \left[\frac{\max(|y_0|, dy_c)^{1/n+1} - \max(|h - y_0|, dy_c)^{1/n+1}}{1/n+1} \right]. \tag{A9}$$

By injecting Eq. (A8) into Eqs. (A7) and (A9) we obtain two equations that are used to calculate y_0 and dy_c for a given flow rate, q, and blade shape, h. The derivative along the curvilinear abscissa, obtained using the relation $\frac{dP}{ds} = \frac{dP}{dx}\sin\theta$, and integrated between s_w and s gives the fluid pressure p, defined as the pressure relative to the atmospheric pressure, $p = P - P_{\text{atm}}$:

$$p(s) = \int_{s_w}^{s} \frac{\partial p}{\partial x}\sin\theta \, ds = \int_{s_w}^{s} \text{sgn}(Vy_0 - q)\frac{1}{dy_c}\frac{\eta_0^{\frac{n}{n-1}}}{k^{\frac{1}{n-1}}}\sin\theta(s')ds' + p_{\text{sw}}, \tag{A10}$$

with p_{sw} the Laplace pressure arising from the presence of a meniscus at $s = s_w$. To obtain an expression of p_{sw}, we model the meniscus by a circular arc which radius of curvature R is determined

from the wetting angles δ_s and δ_b:

$$p_{\text{sw}} = \frac{\gamma}{R} = -\frac{\cos[\delta_b + \pi/2 - \theta(sc)] + \cos \delta_s}{h}\gamma. \tag{A11}$$

Contrary to what can be done for Newtonian fluids, it is not possible to use the value of the pressure at the position $s = L$ to obtain an explicit equation of the flow rate $q = f(h, \theta, p_L, p_{\text{sc}}, V, b, s_w)$. Here the problem is highly nonlinear, so we use solvers to find a value of q, y_0, and dy_c. Once injected in Eq. (A10) at the position $s = L$, they give a pressure at the blade tip approximately equal to its guess p_L.

Finally, the pressure at $s = L$ is determined by considering the pressure at $x = +\infty$ fixed to $P_{\text{atm}} = 0$ and using this condition to solve the shape of the liquid surface after the blade (see Sec. 4 of the Appendix).

Viscous stress. The viscous stress f_v, exerted by the fluid on the blade, is defined as:

$$f_v = -\tau(h) = -\frac{\partial P}{\partial x}(h - yo), \tag{A12}$$

which we now write, using Eq. (A8), as f_v:

$$f_v = -\text{sgn}(Vy_0 - q)\frac{1}{dy_c}\frac{\eta_0^{\frac{n}{n-1}}}{k^{\frac{1}{n-1}}}(h - yo). \tag{A13}$$

Capillary forces. The capillary forces are expressed as:

$$\vec{F}_c = \gamma b \vec{e}_\gamma, \tag{A14}$$

with $\vec{e}_\gamma$ the vector tangent to the free liquid surface at the triple line position.

2. Simplification: Pure shear-thinning fluid under the blade

We observed numerically that taking into account the Newtonian area under the blade has a very limited impact on the results: The pressure profile only differs by less than $10^{-3}\%$ between a simple power-law fluid and the fluid described by Eq. (A3) (with a Newtonian viscosity plateau at low shear). Thus, we used the hypothesis of pure shear-thinning behavior under the blade to speed up the computation. With this simplification, Eq. (A7) becomes

$$q = Vyo - \left\langle\frac{1}{k}\frac{\partial P}{\partial x}\right\rangle^{1/n}\left[\frac{\langle yo\rangle^{1/n+2} + \langle h - yo\rangle^{1/n+2}}{1/n + 2}\right]. \tag{A15}$$

The velocity continuity at y_0 gives:

$$V(1/n + 1) = \left\langle\frac{1}{k}\frac{\partial P}{\partial x}\right\rangle^{1/n}(|yo|^{1/n+1} - |h - yo|^{1/n+1}). \tag{A16}$$

By combining Eqs. (A16) and (A15) we obtain a new equation of the flow rate that depends only on y_0 and h:

$$q = V\left[yo - \frac{1/n + 1}{1/n + 2}\left(\frac{\langle yo\rangle^{1/n+2} + \langle h - yo\rangle^{1/n+2}}{|yo|^{1/n+1} - |h - yo|^{1/n+1}}\right)\right]. \tag{A17}$$

We can express the pressure derivative from Eq. (A15):

$$\frac{\partial P}{\partial x} = k\left\langle\frac{(Vyo - q)(1/n + 2)}{\langle yo\rangle^{1/n+2} + \langle h - yo\rangle^{1/n+2}}\right\rangle^n, \tag{A18}$$

$$p(s) = \int_{\text{sc}}^L k\left\langle\frac{(Vyo - q)(1/n + 2)}{\langle yo\rangle^{1/n+2} + \langle h - yo\rangle^{1/n+2}}\right\rangle^n \sin\theta ds + p_{\text{sw}}. \tag{A19}$$

The viscous stress f_v becomes

$$f_v = -k \left\langle \frac{(V yo - q)(1/n + 2)}{\langle yo \rangle^{1/n+2} + \langle h - yo \rangle^{1/n+2}} \right\rangle^n (h - yo). \tag{A20}$$

3. Torque balance

To solve the blade shape in the large deflection problem, a first step is the calculation of the total external torque $\Gamma(s)$ applied by the fluid on the blade. It corresponds to the sum of all elementary torques applied by the fluid (due to the lubrication force, viscous stress and capillarity) between the working position s and the tip of the blade L. To do so, we need to project the blade angle θ (as defined in Fig. 6) on the x and y axis:

$$\Gamma(s) = b \int_s^L \vec{SS'} \wedge [p(\vec{s'}) + f_v(\vec{s'})] ds' \cdot \vec{u}_z + \vec{SL} \wedge \vec{F}_c \cdot \vec{u}_z \quad (+S\vec{S}_w \wedge \vec{F}_c \cdot \vec{u}_z \text{ if } s < s_w), \tag{A21}$$

$$= b \int_s^L [p[(x(s') - x(s)) \sin \theta(s') - (y(s') - y(s)) \cos \theta(s')] - f_v[(x(s') - x(s)) \cos \theta(s')$$
$$+ (y(s') - y(s)) \sin \theta(s')]] ds' - F_c[(x_L - x(s)) \cos \theta_{mL} + (y_L - y(s)) \sin \theta_{mL}$$
$$+ (x_{sw} - x(s)) \cos \theta_{msw} + (y_{sw} - y(s)) \sin \theta_{msw}]. \tag{A22}$$

θ_{msw} and θ_{mL} are the angles of the tangent of the meniscus with respect to the y axis at the positions $s = s_w$ and $s = L$ respectively.

Since the blade is in an equilibrium position, Euler's elastica implies that the torque produced by the internal stress $E^*I \frac{d\theta}{ds}$ is equal to the total torque $\Gamma(s)$ produced by external forces. Now we write:

$$\Gamma(s) = -E^*I \frac{d\theta}{ds}. \tag{A23}$$

Combining Eqs. (A22) and (A23) gives:

$$\frac{d^2\theta}{ds^2} = \frac{b}{E^*I} \int_s^L [-p \cos(\theta(s) - \theta(s')) + f_v \sin(\theta(s) - \theta(s'))] ds'$$
$$+ F_c[\sin(\theta(s) - \theta_{mL}) + \sin(\theta(s) - \theta_{msw})]. \tag{A24}$$

We finally obtain the equation describing the shape of the blade $\theta(s)$ by replacing p, f_v, and F_c by their expressions [Eq. (A19), (A20), and (A14) respectively].

4. Free surface equations

In a second part, we define a second set of equations to calculate the thickness, shape, and flow in the free liquid film in the 0.8 cm after the tip of the blade. This interval is chosen to be sufficiently large so that the atmospheric pressure is eventually reached into the fluid $p(x = \infty) = 0$. The equations that govern the shape of the free surface are given below and follow an approach discussed by Trinh *et al.* [28]. To distinguish the variables of the free surface from those of the blade we use an index l.

The lubrication equation [Eq. (A2)] is integrated with the boundary condition $\tau(0) = 0$ (no tangential stress on the free surface), which give:

$$\tau = \frac{\partial p}{\partial x}(y - h_l). \tag{A25}$$

Again, we have to consider separately two regions, in which the fluid behaves either as a Newtonian fluid (at low shear rate) or as a power-law liquid (at high shear rate). We define, as before, the boundary between these two regions y_c. Since most of the liquid in the free film is at

rest (with $\dot{\gamma} = 0$), it is particularly important to take into account the Newtonian plateau in the rheological law, contrary to what is done below the blade.

The shear rate equality at y_c gives an expression for the derivative of p:

$$\frac{\partial p}{\partial x} = \text{sgn}\left(\frac{\partial p}{\partial x}\right)\frac{1}{h_l - y_c}\frac{\eta_0^{\frac{n}{n-1}}}{k^{\frac{1}{n-1}}}. \tag{A26}$$

To determine y_c, the no-slip boundary condition on the substrate $[v(0) = V]$ and the velocity continuity at y_c are used to obtain the expressions of the velocity in both regions. The integration gives the flow rate:

$$q_l = Vh_l - \frac{1}{3\eta_0}\frac{\partial p}{\partial x}(h_l - y_c)^3 + \left(\frac{1}{k}\frac{\partial p}{\partial x}\right)^{1/n}\frac{(h_l - y_c)^{1/n+2} - h_l^{1/n+2}}{(1/n + 2)}. \tag{A27}$$

From this equation it can be shown that the sign of $\frac{\partial p}{\partial x}$ is equivalent to the sign of $Vh_l - q_l$. This results leads to a new expression for the pressure derivative:

$$\frac{\partial p}{\partial x} = \text{sgn}(Vh_l - q_l)\frac{1}{h_l - y_c}\frac{\eta_0^{\frac{n}{n-1}}}{k^{\frac{1}{n-1}}}. \tag{A28}$$

The equation describing the flow rate [Eq. (A27)] can be rewritten only as a function of the variables h_l and y_c by using Eq. (A28):

$$q_l = Vh_l - \text{sgn}(Vh_l - q_l)\left(\frac{\eta_0}{k}\right)^{\frac{1}{n-1}}\left[\frac{1}{3}(h_l - y_c)^2 + \frac{1}{(h_l - y_c)^{1/n}}\frac{(h_l - y_c)^{1/n+2} - h_l^{1/n+2}}{(1/n + 2)}\right]. \tag{A29}$$

Since the liquid is incompressible, the flow rate q_l is equal to the flow rate q below the blade. Thus, we use in the numerical resolution of the equations that at $x = \infty$, $q = Vh_l(\infty) = Ve$.

The pressure p in the liquid at the end of the blade is set by the Laplace pressure within the meniscus, which gives a second expression for p:

$$p = -\gamma\frac{d\theta}{ds}. \tag{A30}$$

By combining Eqs. (A30) and (A28), and using the relation between the derivatives with respect to s and x, we finally obtain:

$$\frac{d^2\theta}{d^2s} + \text{sgn}(Vh_l - q_l)\frac{1}{h_l - y_c}\frac{\eta_0^{\frac{n}{n-1}}}{\gamma k^{\frac{1}{n-1}}}\sin(\theta) = 0. \tag{A31}$$

This equation governs the shape of the free surface of the deposited layer of fluid behind the blade. To accelerate of the convergence, the equivalent equation for pure Newtonian fluid is used at s where $y_c = 0$:

$$\frac{d^2\theta}{d^2s} + \frac{3\eta_0}{\gamma}\left(\frac{Vh_l - q_l}{h_l^3}\right)\sin\theta_l(s) = 0. \tag{A32}$$

5. Numerical method

The numerical method used to solve the two sets of equations governing the blade shape and fluid flow is the same as in Ref. [12]. We summarize here what was done.

It is important to notice first that the equations governing the shape of the blade [Eq. (A24)] and the free surface [Eq. (A31)] have the same structure. They can both be written as:

$$\frac{d^2\theta}{d^2s} = -S(s, \theta(s)). \tag{A33}$$

where $-S$ is the right member of Eqs. (A24) and (A31). Interestingly, Eq. (A33) can be seen as a one-dimensional steady-state nonlinear heat equation, where θ is equivalent to temperature and S is a heat source distribution, depending on both s and θ. The heat conductivity is here equal to 1. Following this analogy, we thus solve Eqs. (A24) and (A31) by referring to the transient heat equation [Eq. (A34)], where we add the derivative of θ versus a virtual time t_v, $\frac{\partial\theta}{\partial t_v}$ and a volumetric heat capacity equal to 1,

$$\frac{\partial\theta}{\partial t_v} = \frac{\partial^2\theta}{\partial s^2} + S(s). \tag{A34}$$

The boundary conditions depend on the solved set of equations:

(i) for the hydroelastic equations (the blade and the fluid below) the fixed mounting imposes $\theta(0) = 0$. In addition, since there is no torque at the end of the blade, we also have $\frac{\partial\theta}{\partial s}|_L = 0$.

(ii) for the free surface equations, since the fluid deposited is horizontal far from the tip of the blade (at $x = \infty$), we have $\theta_l(\infty) = \pi/2$. In addition, the Laplace pressure equation written at L imposes: $\frac{\partial\theta_l}{\partial s}|_L = -\frac{p_L}{\gamma}$.

Finally, the matching of the two solutions of Eqs. (A24) (for the blade) and (A31) (for the free film) is done by imposing a continuity of the flow rate q at $x = L$, as well as of the liquid height: $h(x = L) = h_l(x = L)$.

6. Resolution method

The transient heat equation [Eq. (A34)] is solved numerically by finite differences, which gives the asymptotic stationary solution. We start from an initial guess of the shape $\theta(s)$ of the blade. This initial shape is obtained through a rough calculation for a Newtonian fluid (that satisfies the initial guess of the pressure p_L), using the equations of our previous work [12]. The viscosity of this fluid is $\eta = 478$ mPa s and, to facilitate the following calculations, it has the same wetting properties (surface tension, contact angles, and pressure p_{sw}) as the shear-thinning fluid that is studied afterwards.

We chose an implicit-explicit scheme [29,30] as a compromise between stability and computing time. Thus, the source term S is defined explicitly, while θ is not,

$$\frac{\theta_i^{n+1} - \theta_i^n}{\Delta t_v} = \frac{\theta_{i-1}^{n+1} - 2\theta_i^{n+1} + \theta_{i+1}^{n+1}}{\Delta s^2} + S(s, \theta^n), \tag{A35}$$

where $\theta_i^n \approx \theta(i\Delta s, n\Delta t_v)$.

According to the Lax equivalence theorem [31], this scheme is stable and converges to the stationary solution, when it exists. Usually, the timestep Δt_v follows the condition $\Delta t_v < \Delta t_v^{\lim}/2$, where $\Delta t_v^{\lim} = \frac{\Delta s^2}{E^*I}$ and Δs is the size of a cell. However, in most simulations, the model converges nicely so that we can accelerate the calculation, and use instead $\Delta t_v = 20\,\Delta t_v^{\lim}$. For the spatial discretization of the blade equations, we chose to set $\Delta s \in [0.1, 0.5]$ mm. The spacing is nonuniform for the free surface calculation: We increase exponentially the size of the cell from the meniscus area to the "end" of the free film, with Δs increasing from 10^{-5} to 10^{-1} mm.

7. Convergence criteria

For shear-thinning fluids the equation of the flow rate under the blade [Eq. (A17)] requires an additional convergence criteria compared to what is necessary for a Newtonian fluid. Thus, the convergence of the numerical simulation is achieved when three conditions are simultaneously met:

(1) The steady state is reached for the transient heat equation [Eq. (A34)] which provides the solution for the governing equations of the shape of the blade [Eq. (A24)] or the free surface [Eq. (A31)].

(2) The two flow rates, calculated from the blade equations [Eq. (A17)] and from the free film equation [where $q = Vbh_l(\infty)$] equalize (because of flow conservation).

(3) The pressure at L calculated through Eq. (A19) matches the guess value of p_L.

8. Coupling of the blade and free surface calculation

In the resolution process, a given input is the wetting length l_w, which implies that e and l_w both vary quasistatically with time. A new simulation is thus necessary to determine e for each value of l_w. The other inputs are the wetting angles at the position s_w, δ_s, and δ_b (see Fig. 6), whose values are measured experimentally. It is also necessary to make an initial guess of the shape of the blade $\theta(s)$ and of the free surface $\theta_l(s)$ and provide a first estimate of the value of the pressure at the tip of the blade, p_L, as well as the meniscus angle at this position, θ_{mL}. As stated before, the initial guess of $\theta(s)$ is obtained from a rough calculation of the blade shape with a Newtonian fluid, without taking into account the free surface. The shape of free surface is initially modelled as an hyperbolic tangent (to reproduce the meniscus shape). These guesses are used in the computation of the transient heat equations [Eq. (A24)] and [Eq. (A31)], where each step gives an updated $\theta(s)$, $\theta_l(s)$, and $\theta_{mL} = \theta_l(L)$. The arbitrary value of p_L is adjusted through a corrective factor extracted from the difference between the two values of flow rates, q and q_l. This process is iterated until the flow rates can be considered equal, usually within 10^{-4}, leading to the "correct" value of p_L. The fluid thickness e is finally extracted from the height of the deposited fluid for $x \longrightarrow \infty$.

---

[1] Y. Lu, R. Ganguli, C. Drewien *et al.*, Continuous formation of supported cubic and hexagonal mesoporous films by sol–gel dip-coating, Nature **389**, 364 (1997).

[2] Y. Diao, B. K. Tee, G. Giri *et al.*, Solution coating of large-area organic semiconductor thin films with aligned single-crystalline domains, Nat. Mater. **12**, 665 (2013).

[3] A. Lee, P. T. Brun, J. Marthelot *et al.*, Fabrication of slender elastic shells by the coating of curved surfaces, Nat. Commun. **7**, 11155 (2016).

[4] S. Chu, W. Chen, Z. Fang *et al.*, Large-area and efficient perovskite light-emitting diodes via low-temperature blade-coating, Nat. Commun. **12**, 147 (2021).

[5] S. J. Weinstein and K. J. Ruschak, Coating flows, Annu. Rev. Fluid Mech. **36**, 29 (2004).

[6] B. Derjaguin, Thickness of liquid layer adhering to walls of vessels on their emptying and the theory of photo-and motion-picture film coating, Dokl. Acad. Sci. USSR **39**, 13 (1943).

[7] L. Landau and B. Levich, Dragging of a liquid by a moving plate, in *Dynamics of Curved Fronts* (Elsevier, Amsterdam, 1988), pp. 141–153.

[8] J. Seiwert, D. Quéré, and C. Clanet, Flexible scraping of viscous fluids, J. Fluid Mech. **715**, 424 (2013).

[9] J. H. Snoeijer, Analogies between elastic and capillary interfaces, Phys. Rev. Fluids **1**, 060506 (2016).

[10] K. Warburton, D. R. Hewitt, and J. A. Neufeld, The elastic landau–levich problem on a slope, J. Fluid Mech. **883**, A40 (2020).

[11] H. N. Dixit and G. M. Homsy, The elastic landau–levich problem, J. Fluid Mech. **732**, 5 (2013).

[12] M. Krapez, A. Gauthier, H. Kellay, J. B. Boitte, O. Aubrun, J. F. Joanny, and A. Colin, Impact of the Wetting Length on Flexible Blade Spreading, Phys. Rev. Lett. **125**, 254506 (2020).

[13] A. Deblais, R. Harich, A. Colin, and H. Kellay, Taming contact line instability for pattern formation, Nat. Commun. **7**, 12458 (2016).

[14] A. de Ryck and D. Quéré, Fluid coating from a polymer solution, Langmuir **14**, 1911 (1998).

[15] L. Mahadevan and J. B. Keller, Periodic folding of thin sheets, SIAM Rev. **41**, 115 (1999).

[16] J. Ashmore, A. Q. Shen, H. P. Kavehpour, H. A. Stone, and G. H. McKinley, Coating flows of non-newtonian fluids: weakly and strongly elastic limits, J. Eng. Math. **60**, 17 (2008).

[17] R. P. Feynman, R. B. Leighton, and M. Sands, The feynman lectures on physics; vol. i, Am. J. Phys. **33**, 750 (1965).

[18] R. B. Bird, R. C. Armstrong, and O. Hassager, *Dynamics of Polymeric Liquids, Vol. 1: Fluid Mechanics* (John Wiley and Sons Inc., New York, NY, 1987).

[19] T. Sullivan, S. Middleman, and R. Keunings, Use of a finite-element method to interpret rheological effects in blade coating, AIChE J. **33**, 2047 (1987).

[20] A. B. Ross, S. K. Wilson, and B. R. Duffy, Blade coating of a power-law fluid, Phys. Fluids **11**, 958 (1999).

[21] S. Bhatti, M. Zahid, R. Ali, A. Sarwar, and H. A. Wahab, Blade coating analysis of a viscoelastic carreau fluid using adomian decomposition method, Math. Comput. Simul. **190**, 659 (2021).

[22] F. R. Pranckh and L. E. Scriven, Elastohydrodynamics of blade coating, AIChE J. **36**, 587 (1990).

[23] A. E. Hosoi and L. Mahadevan, Peeling, Healing, and Bursting in a Lubricated Elastic Sheet, Phys. Rev. Lett. **93**, 137802 (2004).

[24] P. H. Trinh, S. K. Wilson, and H. A. Stone, An elastic plate on a thin viscous film, arXiv:1410.8558.

[25] A. J. Giacomin, J. D. Cook, L. M. Johnson, and A. W. Mix, Flexible blade coating, J. Coat. Technol. Res. **9**, 269 (2012).

[26] C. M. Corvalán and F. A. Saita, Blade coating on a compressible substrate, Chem. Eng. Sci. **50**, 1769 (1995).

[27] S. P. Timoshenko and J. M. Gere, *Theory of Elastic Stability* (Courier Corporation, North Chelmsford, MA, 2009).

[28] P. H. Trinh, S. K. Wilson, and H. A. Stone, An elastic plate on a thin viscous film, arXiv:1410.8558.

[29] G. D. Smith, *Numerical Solution of Partial Differential Equations: Finite Difference Methods* (Oxford University Press, Oxford, 1985).

[30] S. J. Ruuth, Implicit-explicit methods for reaction-diffusion problems in pattern formation, J. Math. Biol. **34**, 148 (1995).

[31] P. D. Lax and R. D. Richtmyer, Survey of the stability of linear finite difference equations, Commun. Pure Appl. Math. **9**, 267 (1956).